# Proceedings of the Institution of Mechanical Engineers, Part C: Journal of Mechanical Engineering Science

**Contact and elastohydrodynamic analysis of worm gears Part 2: Results**

K. J. Sharif, S Kong, H. P. Evans and R. W. Snidle

The online version of this article can be found at:

Published by:

**⑤SAGE**

On behalf of:

**Institution of MECHANICAL ENGINEERS**

Institution of Mechanical Engineers

# Contact and elastohydrodynamic analysis of worm gears
# Part 2: results

**K J Sharif, S Kong, H P Evans** and **R W Snidle***
Cardiff School of Engineering, Cardiff University, Wales, UK

**Abstract:** The paper presents the results of modelling the contact and elastohydrodynamic lubrication (EHL) effects between the teeth of worm gears. A number of different practical worm gear designs have been studied covering a wide range of sizes and potential applications, from small instrument drives to high power units. All the designs are of the popular ZI type, in which the worm is an involute helicoid, with deliberate mismatch of tooth conformity in order to avoid damaging edge contact. The results cover loaded tooth contact analysis ('loaded TCA') under dry conditions, predicted film-generating behaviour with lubrication, surface and oil film temperatures, and calculated values of friction and transmission efficiency. It is demonstrated that regions of poor film formation may be predicted in a qualitative way on the basis of loaded TCA together with consideration of the kinematics of entrainment at the contacts.

**Keywords:** worm gears, elastohydrodynamic, thermal, non-Newtonian

## NOTATION

| | |
|---|---|
| $a, b$ | Hertzian contact major and minor semi-dimensions (m) |
| $c_0$ | specific heat (J/kg K) |
| $k_0$ | thermal conductivity (W/m K) |
| $S_0$ | lubricant parameter |
| $x$ | Cartesian coordinate in the contact plane (m) |
| $y$ | Cartesian coordinate in the contact plane (m) |
| $Z$ | lubricant parameter |
| | |
| $\varepsilon_0$ | oil thermal expansivity ($K^{-1}$) |
| $\eta_0$ | absolute viscosity at zero pressure (Pa s) |
| $\theta_0$ | reference (bulk, or inlet) temperature (K) |
| $\rho_0$ | density at zero pressure ($kg/m^3$) |
| $\tau_L$ | limiting shear stress (Pa) |
| $\tau_0$ | Eyring shear stress (Pa) |

## 1 INTRODUCTION

Part 1 [1] describes the geometry and kinematics of ZI [2] worm gears and the detailed analysis techniques that have been developed for full modelling of both dry

elastic contact (tooth contact analysis or TCA) and elastohydrodynamic lubrication (EHL) between the teeth, utilizing a full thermal treatment and incorporating non-Newtonian rheological behaviour of the lubricant. In the ZI system the worm takes the form of an involute helicoid and in traditional practice a hob of the same form and size as the worm is used to generate a matching conjugate wheel. In most modern designs, however, including those considered here, a deliberate mismatch is introduced between the curvature of the worm teeth and that of the mating wheel. Instead of conjugate line contact between the teeth, there is localized non-conforming contact, which is nominally at a single point under zero load conditions. The geometry is achieved by cutting the gear wheel with a hob of slightly different (or 'oversize') form to that of the worm. This procedure, while nominally reducing the conformity of the teeth and hence increasing the contact stress, has the major advantage of introducing a degree of self-alignment, thereby eliminating the more damaging stress-raising edge contacts which are inevitable when otherwise closely conforming bodies become slightly misaligned. The degree of mismatch introduced by the gear designer represents a practical compromise between tolerance of manufacturing and setting errors on the one hand and contact stress on the other. Mismatch also introduces a converging 'inlet' to the contact which, it is generally agreed, improves entrainment of oil and lubrication performance (although the term 'inlet' may

be less than wholly appropriate, as can be seen from the discussion in later sections.)

Because of the high degree of sliding present in worm gears, it is almost universal practice to make the wheel of a relatively soft material relative to that of the worm (which is usually of hardened steel) in order to prevent heavy adhesive wear and seizure. Bronze (either phosphor or leaded) is the most widely used wheel material, and, if serious abrasive wear and fatigue pitting are to be avoided, this limits the allowable maximum contact pressure to values far lower than those found in conventional steel/steel gearing. In the results presented here, a 600 MPa maximum dry contact pressure has been regarded as a reasonable upper limit for a steel/bronze worm pair in practice.

## 2   DESIGNS CONSIDERED

Eight different worm gears have been considered in this study, ranging from a small instrument drive to a large power unit. The design parameters of the worm/wheel pairs are summarized in Table 1. All units are manufactured with an 'oversize' hob which gives a localized point contact under zero load. Six of the designs have worms having a single tooth (described as 'single-start') and the remaining two units have three and four-start worms. The range of sizes considered is illustrated schematically in Fig. 1 which shows the smallest and largest of the eight designs considered, drawn to the same scale and giving the numbers of teeth on the worm and wheel. The designs are labelled A to H for convenience. The zero load gap between the tooth surfaces at three stages of the meshing cycle is illustrated in Figs 2 and 3 for two designs of different scale and giving rise to significantly different gap contours. Figure 2 shows the gap contours for the small single-start design A at three positions corresponding to contact at the wheel root, mid-tooth and wheel tip respectively. It should be noted that figures of this type show contours and tooth edges projected into the common tangent $(x, y)$ plane at the point of contact. Contact is delimited by the edges of the wheel teeth in the $x$ direction and by the worm tip in the upward direction and by the wheel tip in the downward direction. (The stepped nature of the contours at some of the boundaries is a consequence of specifying large values of the gap outside the region where both teeth are present. All contours that reach tooth boundaries are open contours.) The curved recess at the lower edge corresponds to the wheel tip clearance throat. There is a clear tendency for the gap contours to become more elongated when contact is at the wheel root. Figure 3 shows similar contours for the much larger four-start design (H). In this case the contours are more elongated and less symmetrical in shape. As explained in Part 1, the gap geometry under zero load is obtained from geometrical analysis using the program

devised by Hu [3]. This information, together with kinematic analysis to give the entrainment velocity pattern, is the starting point for subsequent contact and elastohydrodynamic modelling.

## 3   MATERIALS AND LUBRICANTS

The traditional material combination used in ZI worm gear practice is steel/bronze, and the relevant elastic and thermal properties of these two materials are shown in Table 2. The exact properties of bronze depend upon the alloy composition: the values shown in Table 2 are typical of a commonly used phosphor bronze. Lubricants for use in worm gears are usually of relatively high viscosity and are specially formulated to cope with the high sliding tooth contacts. In modern practice there is a preference for synthetic polyglycol oils with antiwear chemical additive packages. The EHL analysis presented here is concerned only with the hydrodynamic performance of the lubricant, and the properties of relevance are the physical and rheological parameters. The polyglycol oil selected for analysis is of ISO 460 viscosity grade. This oil has been used in a parallel experimental study of worm performance at Newcastle University. The parameters describing the viscosity/temperature/pressure characteristic together with the shear thinning and limiting shear stress behaviour have been determined as described in reference [1] on the basis of figures given by Larsson *et al.* [4], and are summarized in Table 2. The results given in the present paper correspond to an Eyring shear thinning rheological model.

## 4   DRY ELASTIC CONTACT

The aim of dry elastic contact simulation is to show the size and area of the loaded contact between the teeth in relation to the edges of the teeth and the contact pressures present. This process is often described as loaded tooth contact analysis (loaded TCA). The exact simulation of the contact of worm gears is complicated by the fact that load is shared between a number of simultaneous tooth engagements (typically two or three in number). The way in which the total load is distributed at these contacts depends on tooth bending stiffness, alignment and the accuracy of spacing of the teeth (pitch error). Clearly, therefore, any exact prediction of contact behaviour must involve a complicated structural analysis that takes account of these factors in a given situation. Such analyses have been carried out (see, for example, reference [5]), but for basic sizing purposes the designer requires a simpler approach based on some assumed sharing or the worst case of single-tooth contact. In the following results it is assumed that the tooth contact load is known. The undeformed geometry of the tooth surfaces is used to perform a non-Hertzian elastic

**Table 1** Worm/wheel design parameters

| | Design A | Design B | Design C | Design D | Design E | Design F | Design G | Design H |
|---|---|---|---|---|---|---|---|---|
| Number of worm threads | 1 | 1 | 1 | 1 | 1 | 1 | 3 | 4 |
| Worm tip radius (mm) | 8.48 | 9.97 | 13.21 | 32.47 | 33.33 | 63.5 | 48.01 | 65.00 |
| Worm root radius (mm) | 6.15 | 6.00 | 7.44 | 21.53 | 18.78 | 35.79 | 29.03 | 44.32 |
| Worm base radius (mm) | 1.42 | 2.37 | 3.41 | 6.63 | 8.60 | 16.39 | 26.23 | 35.00 |
| Worm axial pitch (mm) | 3.33 | 5.71 | 8.31 | 15.70 | 20.94 | 39.90 | 28.73 | 31.41 |
| Worm lead (mm) | 3.33 | 5.71 | 8.31 | 15.70 | 20.94 | 39.90 | 86.18 | 125.66 |
| Worm base lead angle (deg) | 20.40 | 20.94 | 21.19 | 20.64 | 21.18 | 21.18 | 27.61 | 29.74 |
| Number of wheel teeth | 70 | 40 | 40 | 50 | 40 | 60 | 59 | 51 |
| Wheel face width (mm) | 8.20 | 11.48 | 15.86 | 35.56 | 46.00 | 88.90 | 60.33 | 69.28 |
| Wheel tip radius (mm) | 38.62 | 38.99 | 56.86 | 132.50 | 143.23 | 399.86 | 278.61 | 268.50 |
| Wheel throat radius (mm) | 38.09 | 38.09 | 55.54 | 130.86 | 140.20 | 393.52 | 274.03 | 263.80 |
| Hob tip radius (mm) | 9.96 | 11.61 | 15.00 | 33.63 | 35.30 | 70.18 | 51.63 | 67.39 |
| Hob root radius (mm) | 7.63 | 7.63 | 9.23 | 22.68 | 20.80 | 40.77 | 31.58 | 46.72 |
| Hob base radius (mm) | 1.43 | 2.40 | 3.45 | 6.65 | 8.60 | 16.47 | 26.48 | 35.27 |
| Hob lead (mm) | 3.32 | 5.70 | 8.30 | 15.69 | 20.94 | 39.87 | 85.97 | 125.34 |
| Hob axial pitch (mm) | 3.32 | 5.70 | 8.30 | 15.69 | 20.94 | 39.87 | 28.66 | 31.34 |
| Hob base lead angle (deg) | 20.29 | 20.71 | 20.95 | 20.59 | 21.18 | 21.08 | 27.33 | 29.49 |
| Hob/wheel centre distance (mm) | 45.72 | 45.72 | 64.77 | 153.54 | 161.00 | 434.29 | 305.62 | 310.52 |
| Worm/wheel centre distance (mm) | 44.45 | 44.45 | 63.5 | 152.4 | 160.00 | 431.80 | 304.8 | 310.00 |
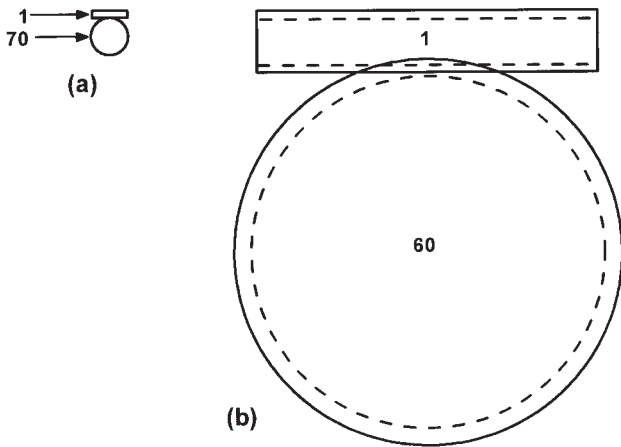
**Fig. 1** Schematic illustration of the range of worm gear sizes considered: (a) design A; (b) design F (figures show numbers of teeth on each component)

contact simulation that takes account of the non-symmetrical nature of typical contact contours as shown in Fig. 3.

Contact simulation may be carried out at any stage of meshing. Figure 4 shows the dry contact area at the nominal mid-mesh position for the eight different designs considered. The load applied in each case is that which leads to a maximum contact pressure of approximately 600 MPa during the meshing cycle. In this case the contact and the edges of the teeth are projected into a plane parallel to the wheel axis. A striking feature of these results is that the aspect ratio of the contact area is significantly more elongated than the gap contours in the corresponding unloaded case. The non-symmetrical nature of the contact also becomes more apparent. Table 3 compares the maximum contact pressure and overall contact dimensions of the results shown in Fig. 4 with the corresponding equivalent Hertzian values based on the principal radii of relative
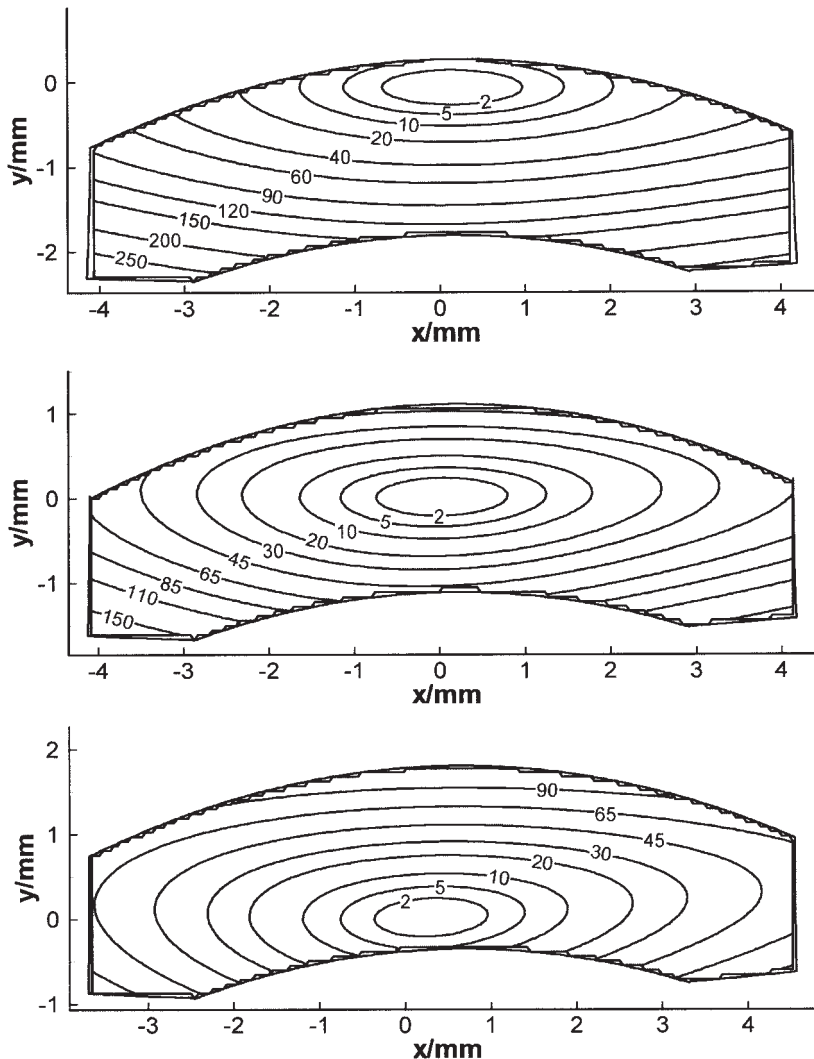


**Fig. 2** Contours (μm) of the gap between worm and wheel teeth at zero load at three stages of the meshing cycle (design A)
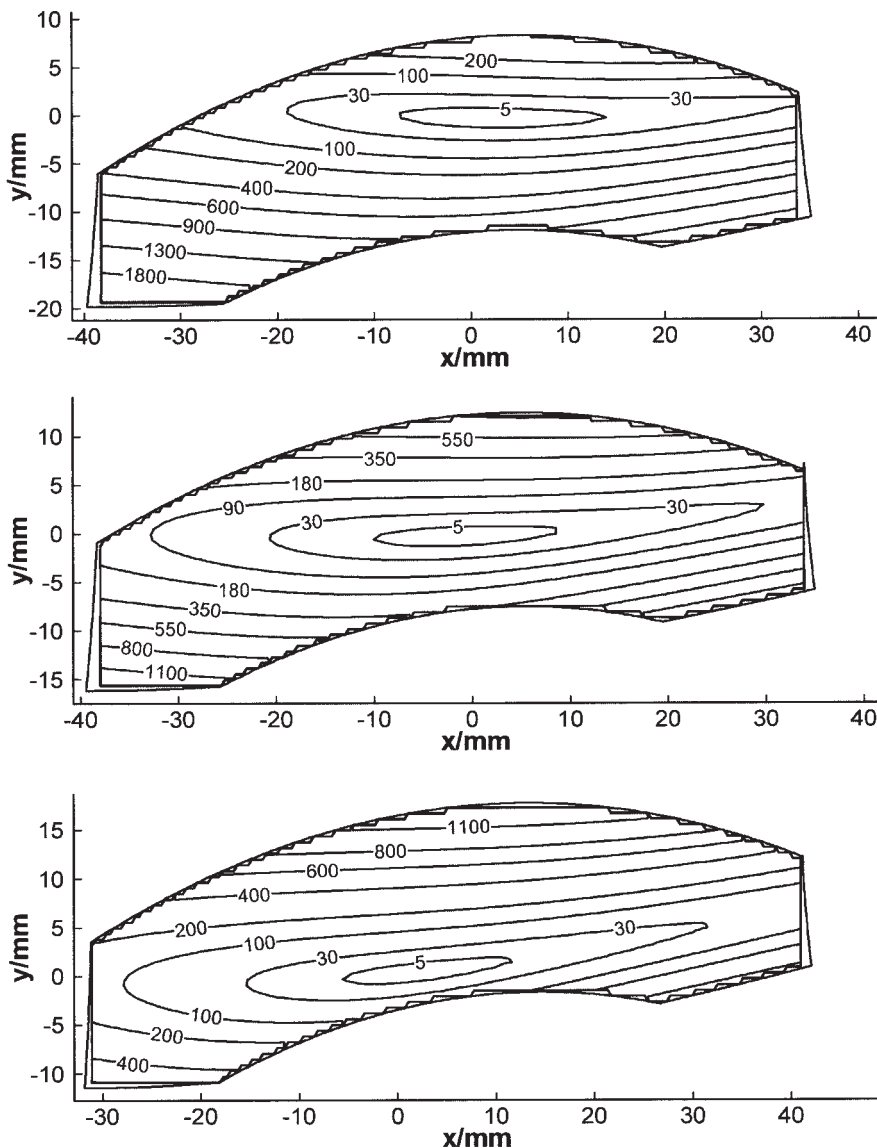
**Fig. 3**   Contours (μm) of the gap between worm and wheel teeth at zero load at three stages of the meshing cycle (design H)

curvature of the unloaded surfaces at the point of contact. In general it may be seen that the contact pressure from Hertz theory is within about 1.5 per cent of the non-Hertzian values and the contact dimensions typically differ by about 4 per cent, with a difference of up to 13 per cent in the major dimension while the difference in the minor dimension ranges from less than 1 per cent up to 13 per cent. The asymmetry in the non-Hertzian results can be quite marked, however, leading to a difference of as much as 24 per cent in the distance from the nominal contact point to its longitudinal boundary in the two directions.

An illustration of the 'footprint' area swept by the contact over the whole meshing cycle is shown in Fig. 5 for the two designs shown earlier. These results emphasize a difference between a single-start and mul-

tistart design: in the four-start design there is far greater movement of the contact across the wheel tooth during the meshing cycle. Deliberate mismatch of the worm and wheel ensures that the contact does not encroach upon the side edges of the wheel tooth, but the tips of both wheel and worm are reached. The consequences of this are severe in terms of local contact stress, as illustrated in Fig. 6 which shows the contact pressure surface and corresponding contact area for wheel tip, middle of tooth and worm tip contact for design G. The very severe stress concentration caused by the contact running over the tooth edges is clearly to be avoided in practice, if possible by correct application of an appropriate degree of tip relief on both worm and wheel. (Note that for the wheel tip case the pressure plot is viewed from the wheel axis side for clarity.)

**Table 2** Worm/wheel operating conditions, material properties, and lubricant properties

| | | |
|---|---|---|
| *Operating conditions* | | |
| Worm input speed (r/min) | 1500 | |
| Nominal maximum contact pressure (MPa) | 600 | |
| | | |
| *Material properties* | | |
| | Worm | Wheel |
| Modulus of elasticity (GPa) | 207 | 120 |
| Poisson's ratio | 0.3 | 0.35 |
| Density (kg/m$^3$) | 7900 | 8800 |
| Thermal conductivity (W/m K) | 47 | 52 |
| Specific heat (J/kg K) | 477 | 420 |
| | | |
| *Lubricant properties* | | |
| Inlet temperature $\theta_0$ (°C) | 60 | |
| Inlet viscosity $\eta_0$ (Pa s) | 0.227 | |
| Inlet density $\rho_0$ (kg/m$^3$) | 1025 | |
| Lubricant parameter $Z$ | 0.227 | |
| Lubricant parameter $S_0$ | 0.782 | |
| Equivalent pressure viscosity coefficient at 60°C (GPa$^{-1}$) | 9.5 | |
| Eyring shear stress $\tau_0$ (MPa) | 3 | |
| Limiting shear stress $\tau_L$ (MPa) | 300 | |
| Thermal expansivity $\varepsilon_0$ (K$^{-1}$) | $7.1 \times 10^{-4}$ | |
| Thermal conductivity $k_0$ (W/m K) | 0.148 | |
| Specific heat $c_0$ (J/kg K) | 1844 | |

## 5   ELASTOHYDRODYNAMIC LUBRICATION

The formulation of the basic equations of elastohydrodynamic lubrication for application to worm gear contacts is described in Part 1. The main features of an EHL worm contact that call for special attention are:

(a) its point contact geometry;
(b) variation in the entrainment direction throughout the contact owing to spin motion of the worm, as shown in Fig. 7 for designs A and H considered earlier;
(c) a high degree of sliding which causes high shear rates in the lubricant in the load-bearing region;
(d) significant thermal effects.

The EHL model that has been used responds to all of these requirements and can be used to predict oil film thickness and pressure distribution together with gear surface and oil film temperatures and friction. The operating conditions selected for presentation represent the extreme of loading which is taken to be determined by a maximum elastic contact pressure of approximately 600 MPa during the meshing cycle. A constant worm speed of 1500 r/min has been taken as representative of many industrial drives.

Table 4 summarizes the main results obtained from the thermal EHL analysis for the eight different worm designs. The normal load figure is chosen to give the approximate target maximum dry pressure of 600 MPa. Under the heavily deformed conditions of the EHL contact, the maximum fluid film pressure is approximately equal to this value. The minimum film thickness is the minimum value occurring within the contact region and the central value is that at the position of the nominal point of contact under dry unloaded conditions. The efficiency of power transfer is calculated as the ratio of total frictional power to that transmitted at the tooth contact. The higher calculated mesh efficiency figures for the larger designs are due mainly to the reduction in viscosity brought about by the high temperatures that result from the higher sliding velocities.

Detailed results from the thermal EHL analysis for the two designs considered earlier are shown in Figs 8 to 10. Figure 8 shows the pressure distributions and indicates that the hydrodynamic pressure distribution is effectively limited to the dry contact area with pressure building up sharply over a relatively short length of the available inlet region. This behaviour is typical of a 'heavily deformed' EHL contact in which the nominal oil film thickness is very small compared with the elastic deflection at the contact. Figure 9 shows the film thickness and temperature contours for design A with contact roughly half-way up the wheel tooth. Owing to the small scale of this design, the velocity of sweep across the wheel tooth is relatively low which gives rise to a minimum film of only 0.12 μm. The localized nature of the contact combined with a relatively low aspect

**Table 3** Summary of results from dry elastic contact simulation

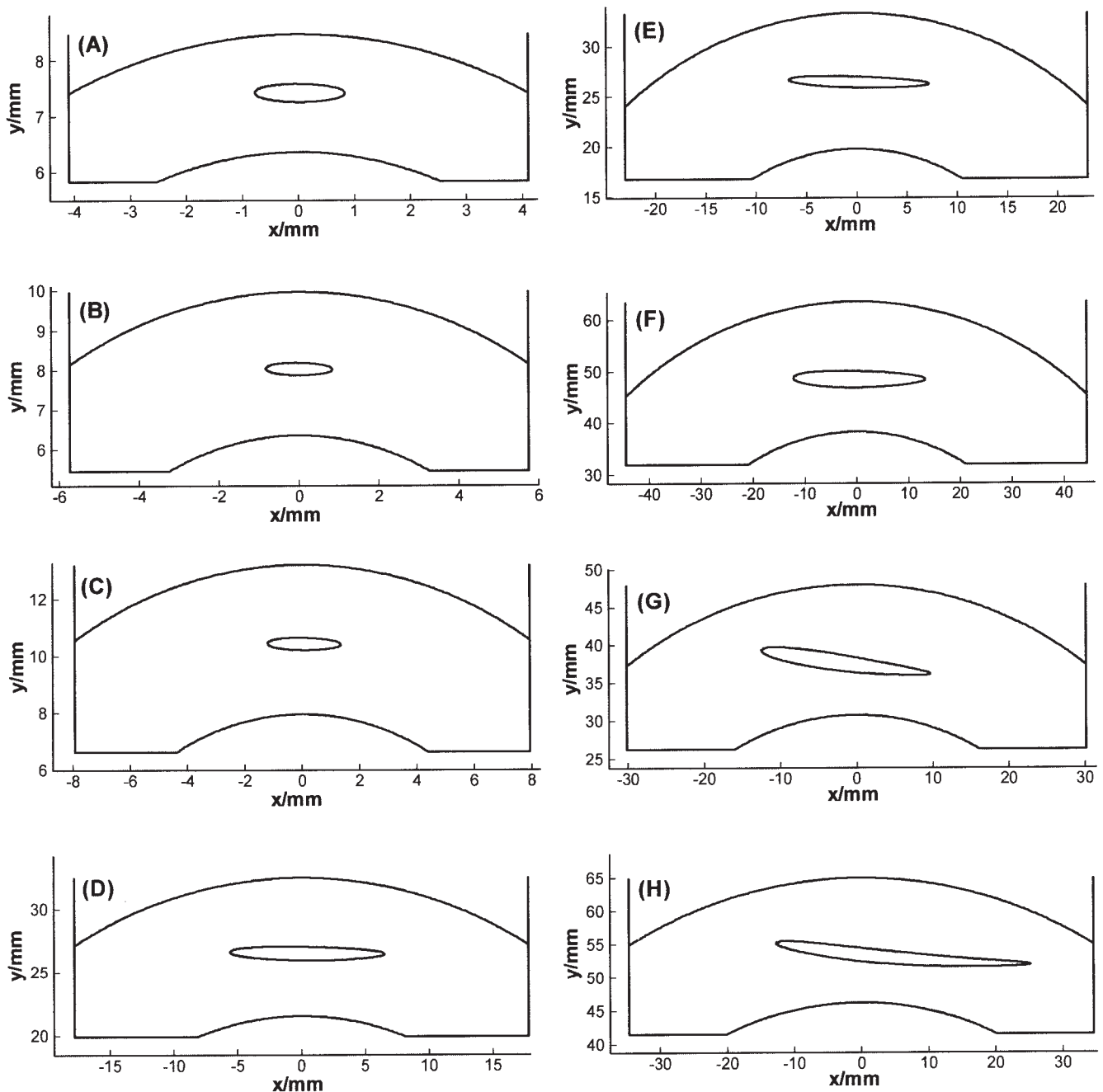| | Results from dry contact simulation | | | Results from Hertzian theory | | |
|---|---|---|---|---|---|---|
| Design | $P_{max}$ (MPa) | $2a$ (mm) | $2b$ (mm) | $P_0$ (MPa) | $2a$ (mm) | $2b$ (mm) |
| A | 569 | 1.64 | 0.35 | 570 | 1.53 | 0.31 |
| B | 541 | 1.73 | 0.31 | 542 | 1.63 | 0.28 |
| C | 534 | 2.60 | 0.46 | 535 | 2.46 | 0.42 |
| D | 552 | 12.15 | 1.14 | 554 | 11.68 | 1.09 |
| E | 548 | 14.11 | 1.18 | 551 | 13.32 | 1.12 |
| F | 584 | 26.12 | 3.37 | 588 | 25.13 | 3.36 |
| G | 540 | 23.33 | 2.39 | 548 | 20.65 | 2.36 |
| H | 510 | 40.51 | 2.15 | 515 | 36.55 | 2.13 |

**Fig. 4** Area of dry elastic contact determined from contact simulation for each of the eight designs at approximate mid-mesh position. Loads and corresponding stresses are given in Table 4. (In this and similar figures, x and y are global axes with x parallel to the wheel axis)

ratio of the contact produce an almost symmetrical film shape with the two thin film side lobes characteristic of a conventional elliptical EHL contact with longitudinal entrainment. The temperature contours show a maximum rise above the inlet reference value of about 15 K. The significant difference in behaviour of the tooth surface temperatures may be noted. The worm surface, which moves roughly from left to right relative

to the contact, has a temperature 'wake' to the right of the contact, but the wheel surface, which moves in the perpendicular direction, has its temperature wake below the contact. The more elongated contact of design H has a strikingly different EHL behaviour, as seen in the film thickness contours of Fig. 10. The larger scale of this design (but running at the same rotational speed as design A) gives a higher entrainment
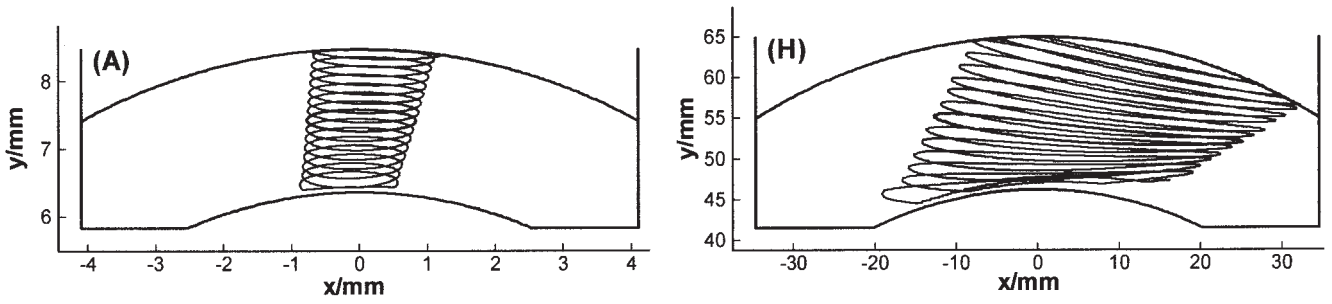
**Fig. 5** Illustration of the area of dry contact swept out during meshing for the two designs A and H
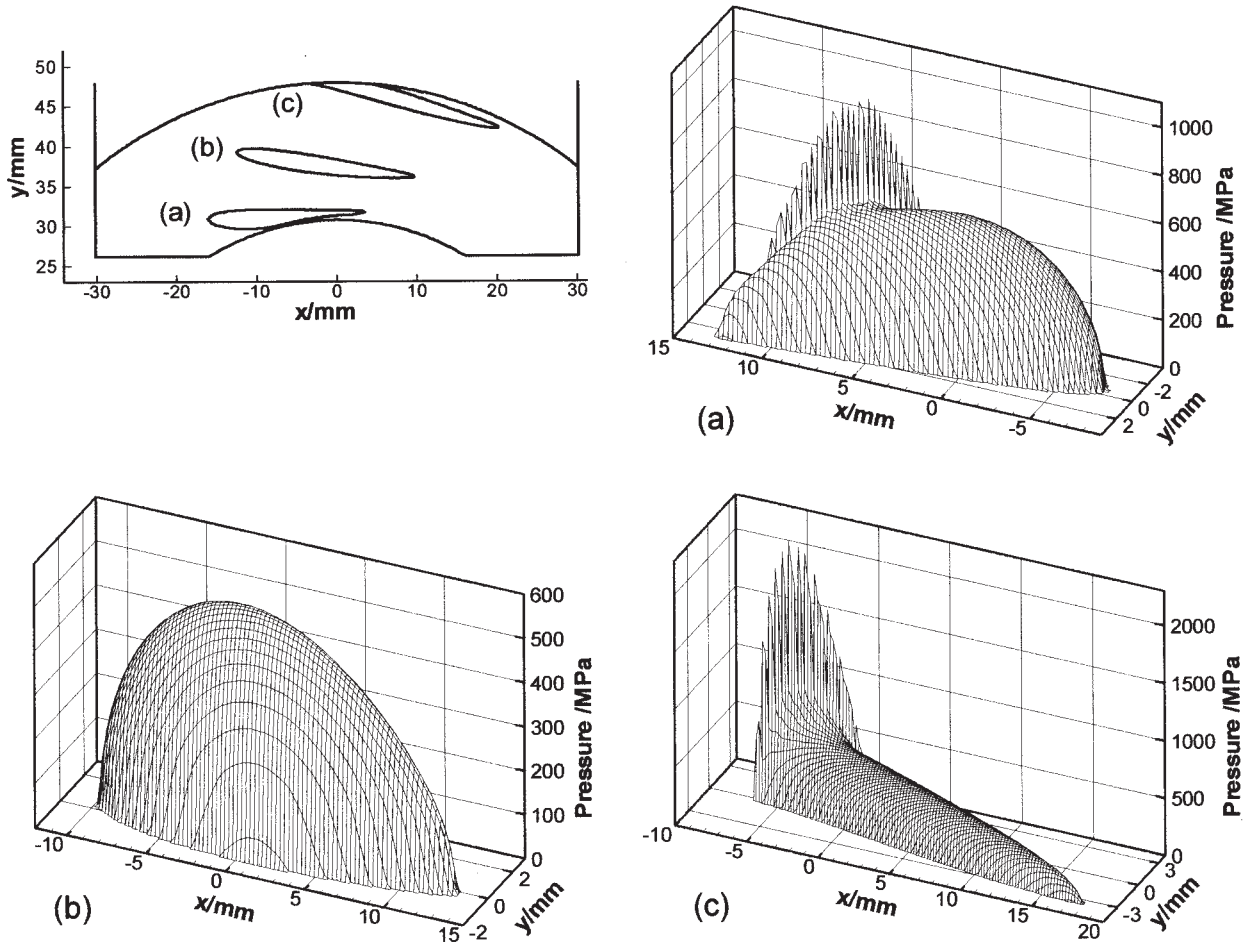


**Fig. 6** Dry elastic contact pressure surfaces at three stages of meshing for design G, illustrating the effect of edge contact: (a) contact at wheel tooth tip; (b) contact at approximately mid-mesh position; (c) contact at worm tip

velocity and a significantly thicker minimum film of 0.39 μm. The film contours are seen to be unsymmetrical. The upper of the two thin film areas has been spread across the contact area by the rotational motion of the worm so as to divide the overall contact into two

parts. This feature is described in detail in Part 1 [**1**] and arises as a result of the rotational entrainment velocity field (illustrated in Fig. 7), leading to two distinct entrainment regions being developed. The part of the dry contact area contact below the upper thin
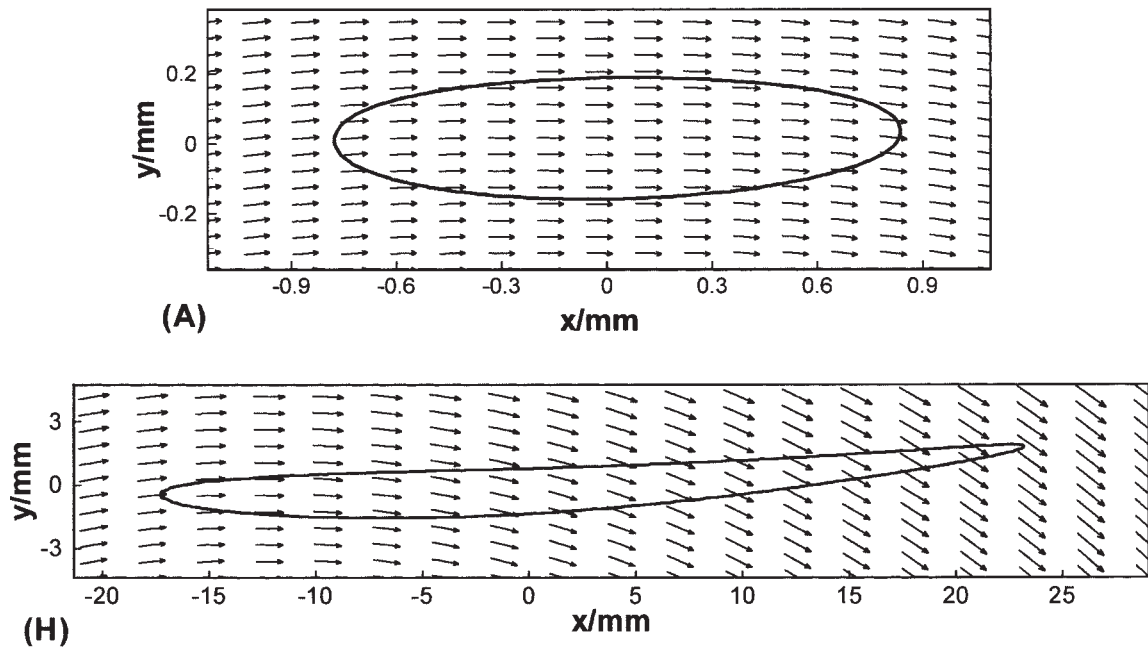
**Fig. 7** Entrainment vectors at approximate mid-mesh position in relation to the dry elastic contact area for the two designs A and H

**Table 4** Summary of results of EHL analysis of worm gear designs

| Design | Normal load on tooth (N) | Minimum film thickness (μm) | Central film thickness (μm) | Maximum pressure (MPa) | Maximum temperature on worm (°C) | Maximum temperature on wheel (°C) | Maximum temperature in oil film (°C) | Efficiency of power transfer (%) |
|--------|-----|------|------|-----|-------|-------|-------|------|
| A | 140 | 0.12 | 0.26 | 598 | 73.2 | 75.4 | 75.5 | 78.2 |
| B | 130 | 0.11 | 0.24 | 567 | 73.7 | 75.5 | 75.9 | 84.2 |
| C | 290 | 0.14 | 0.33 | 559 | 76.3 | 78.6 | 79.5 | 87.3 |
| D | 3700 | 0.22 | 0.56 | 570 | 103.1 | 106.1 | 109.8 | 85.8 |
| E | 4300 | 0.22 | 0.54 | 563 | 103.6 | 104.8 | 109.2 | 89.1 |
| F | 26 000 | 0.43 | 1.33 | 599 | 116.7 | 123.2 | 133.4 | 93.7 |
| G | 14 000 | 0.29 | 0.88 | 547 | 107.6 | 105.5 | 116.8 | 96.6 |
| H | 21 000 | 0.39 | 0.51 | 483 | 122.9 | 118.6 | 134.5 | 96.4 |

film region in Fig. 10 is supplied with lubricant entrained from the bottom left-hand area of the overall contact, whereas the part above the upper thin film region is supplied with lubricant entrained from the top right of the overall contact. The thin film boundary between these regions corresponds in location to the shoulder-like feature seen in the EHL pressure distribution of Fig. 8b which is not seen in the corresponding dry contact calculation. Figure 10 also shows that far higher temperatures are generated for design H because of the faster sliding with maximum worm, wheel and oil film temperatures of 123, 119 and 135 °C respectively. In contrast to design A, it is seen that significant solid convection of temperature by the wheel tooth into the primary inlet of the contact takes place. This is an unusual feature of worm contacts which tends to produce a thinning effect usually absent in contacts in which both surfaces move in generally the same direction.

The regions of severe film thinning sweep out a spiral path over the worm surface during the meshing cycle and move across the wheel tooth from tip to root. They are likely to be associated with significant wear of the softer wheel surface in practice. It is therefore of interest to show the region of film thinning generated upon the wheel surface during the meshing cycle. Figure 11 shows a wheel tooth with the two regions of film thinning determined from each of the three EHL solutions obtained for this design superimposed. The envelope of these regions is suggested as the corresponding band of wear to be expected in practice.
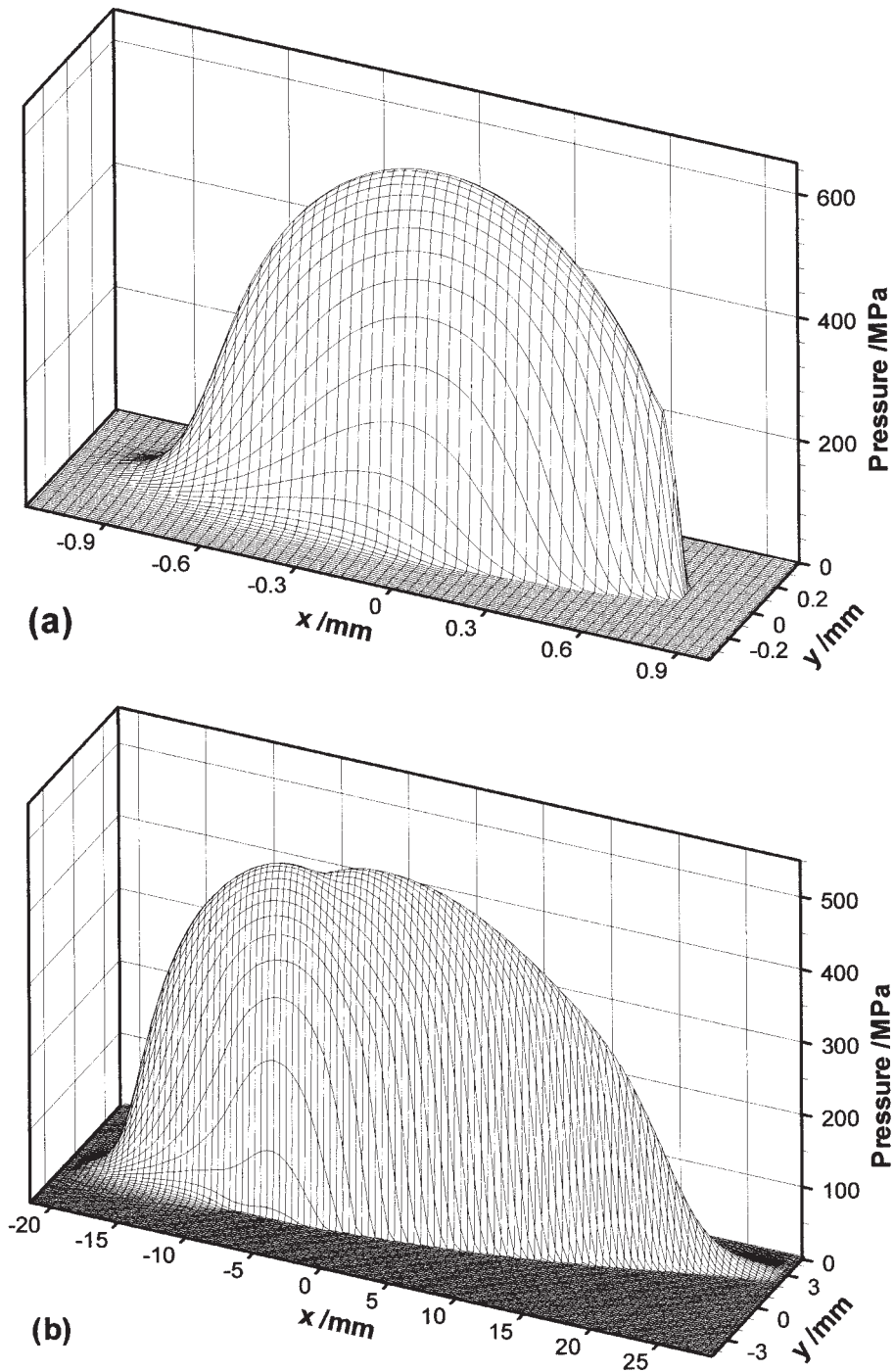
**Fig. 8**  Elastohydrodynamic pressure distributions: (a) design A; (b) design H. Primary inlet to the contacts is on the left

## 6  PREDICTION OF POOR FILM FORMING FROM DRY CONTACT

It is a feature of EHL point contacts that, within the main load-bearing thin film part of the contact (cor-

responding roughly to the equivalent Hertzian region), flow of the lubricant is dominated by the motion of the surfaces (Couette flow) and, because of the combination of a thin film and the tremendously pressure-increased viscosity, the pressure-induced flow (Poi-
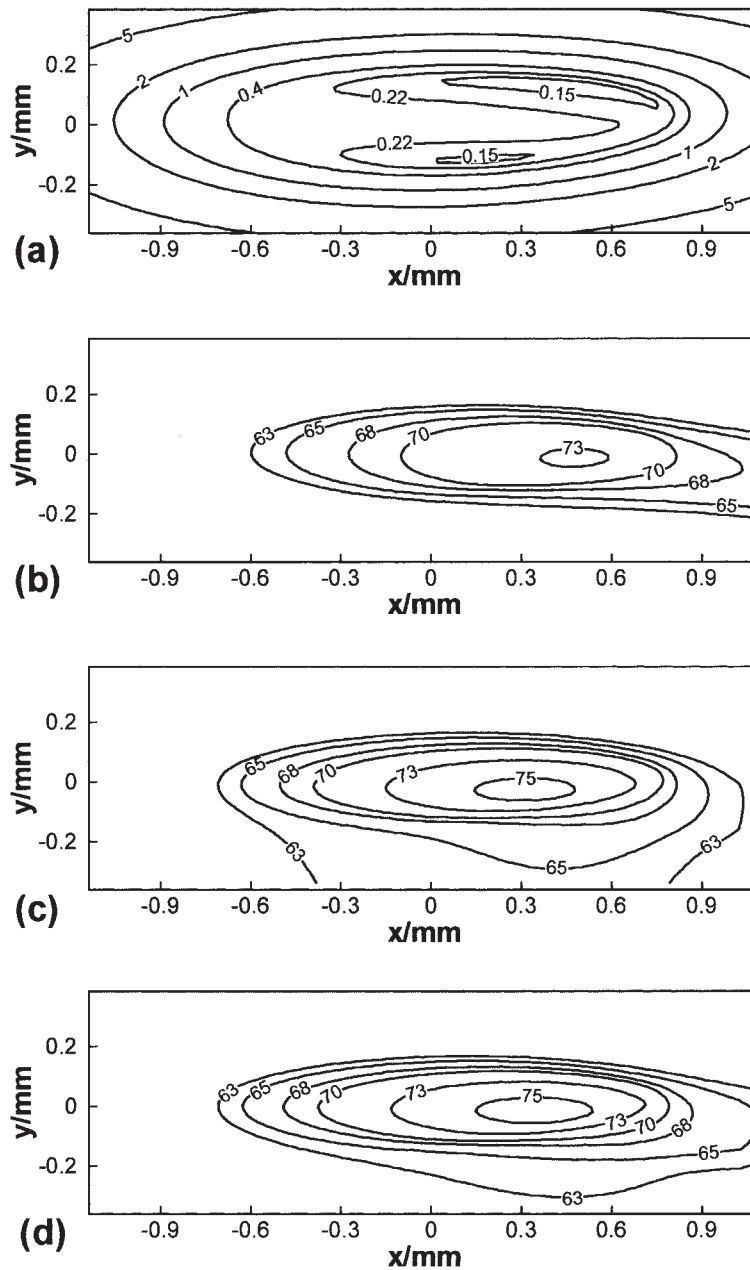
**Fig. 9**  (a) Elastohydrodynamic film thickness contours ( μm); (b) worm surface temperature contours (°C); (c) wheel surface temperature contours (°C); (d) oil mid-film temperature contours (°C). Design A

seuille flow) is negligible. Oil entrained into this region will therefore follow the entrainment streamlines, and these may be determined from purely kinematic considerations as described in Part 1. It also follows that at points where entrainment lines are tangential to the edge of the high-pressure (roughly Hertzian) region there will be zero net entrainment of oil into the contact at the tangency point, and this should therefore indicate a line of poor film formation. This

hypothesis may be examined by comparing the film contours for some different cases of worm contacts considered in this paper with their corresponding entrainment streamlines. This comparison is given in Fig. 12 which shows film contours for designs A, D, F and H with corresponding dry contact areas determined from elastic contact simulation together with superimposed entrainment lines labelled A and B that are tangential to the edge of the contact. The striking
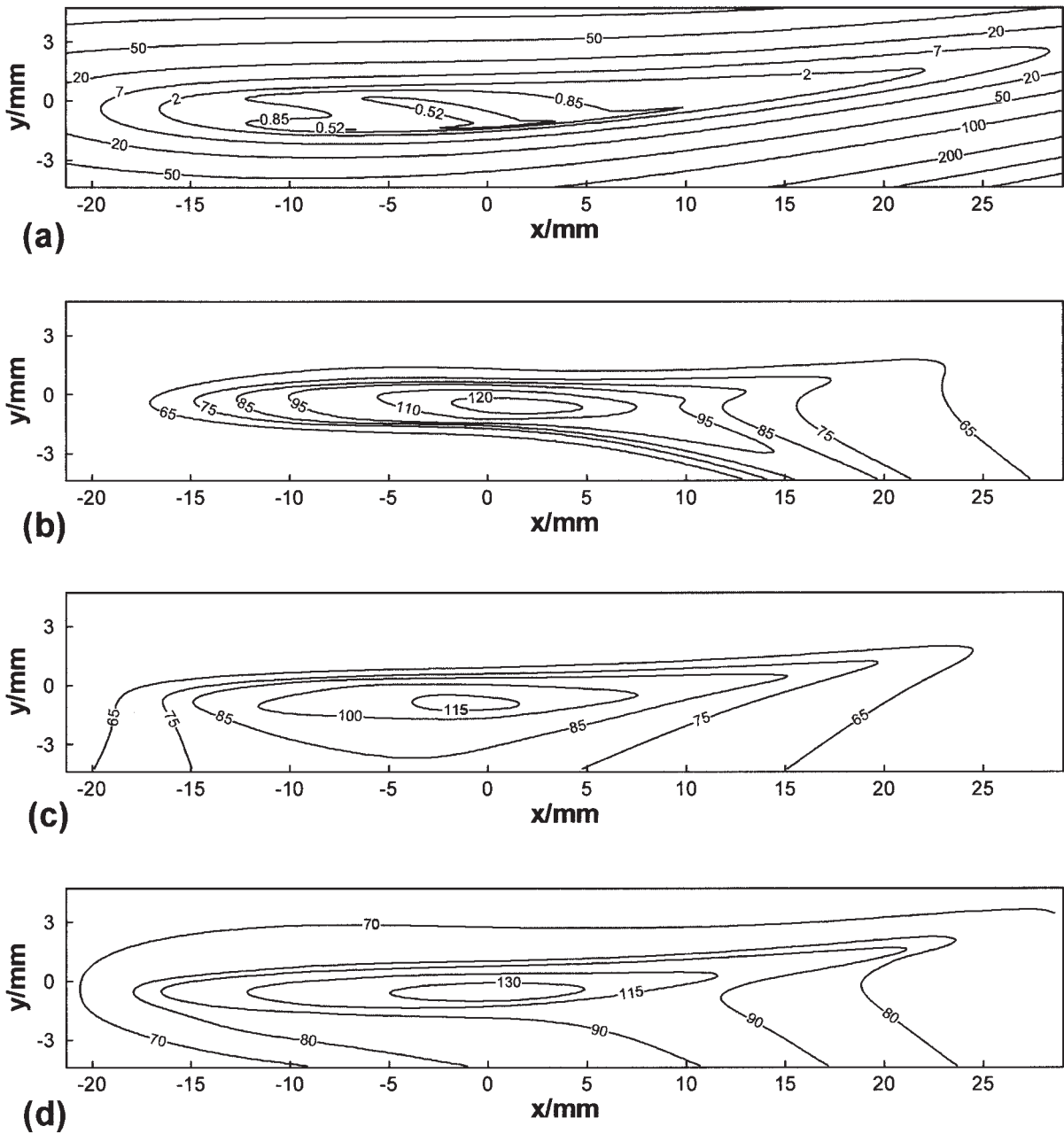
**Fig. 10** (a) Elastohydrodynamic film thickness contours (μm); (b) worm surface temperature contours (°C); (c) wheel surface temperature contours (°C); (d) oil mid-film temperature contours (°C). Design H

similarity between the regions of severe film thinning and the path of tangential entrainment streamline A within the contact is clear, and it can be seen that the entrainment line downstream of point A is an unentrained region.

## 7 DISCUSSION AND CONCLUSION

The results shown in this paper demonstrate that the techniques described in the companion paper may be used to predict the contact and lubrication behaviour of

a wide range of real worm gear designs of the ZI type. Loaded TCA analysis taking account of the strictly non-Hertzian geometry of the tooth contacts shows the small degree of error introduced when the Hertzian assumption is made. In the designs considered, this amounts to a maximum error of 1.5 per cent on contact pressure and 13 per cent on contact dimension. The Hertz equations may therefore be used with some confidence for the prediction of contact pressure and stresses in worm contacts of the type considered. The contact dimensions are also reasonably well predicted by the Hertz equations. The greatest discrepancy between the Hertzian
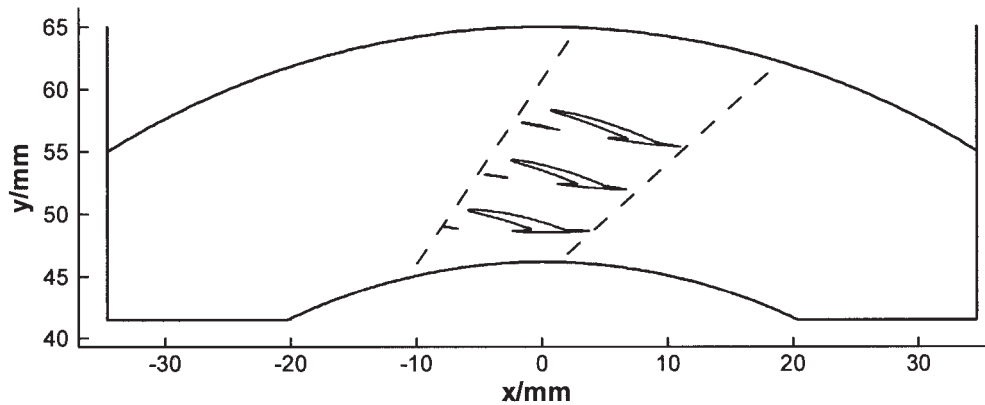
**Fig. 11** Illustration of the region of potential wear on the surface of the wheel tooth as predicted from regions of poor film forming (design H). Contour values are approximately 0.5 μm

and numerically obtained contacts is for design H which gives rise to a significantly asymmetric geometry, as may be seen in Fig. 4. The detailed predictions of the contact for design H using the two methods are shown in Fig. 13. This comparison shows that, although the overall dimensions of the two contacts are closely similar, the predicted *position* of the contact on the tooth flanks is significantly affected by the asymmetry of the contact geometry.

The detailed comparison of the EHL analysis has quantified the suspected poor film forming of these devices by predicting minimum films of the order of 0.5 μm or less with the high-viscosity lubricant used in the study. The main features of the contacts considered are an elongated asymmetrical shape which tends to give relatively poor film generation owing to entrainment mainly in the longitudinal direction, and, in most cases, division of the contact into two regions separated by a band of severe thinning.

The film thickness values obtained from the full thermal EHL analyses are compared with estimates made by the use of the formulae presented by Chittenden *et al.* [6] for elliptical contacts with entrainment at any angle to the ellipse axes in Tables 5 and 6. These formulae were used in two ways, firstly using the entraining velocity at the contact point together with the principal radii of relative curvature at the same location (denoted $CDDT_1$), and secondly taking the entrainment angle to be that at the inlet edge of the corresponding dry contact (denoted $CDDT_2$). The formulae are found to overestimate film thickness in each case, with percentage differences between the model results and those of the formulae varying from 40 per cent to over 300 per cent. The average difference for the eight designs is around 110 per cent. The formulae of Chittenden *et al.* are based on Newtonian isothermal conditions, so it is to be expected that they will give significantly thicker film predictions than those calculated in this high sliding application. A further limitation of these formulae in this application is that they were derived from results at

radius ratios of up to about 6, whereas the nominal ratios for the worm contacts considered here vary from 12 to 90.

Adjustment of design parameters with the objective of ensuring that the contact is enclosed between the entrainment streamlines A and B identified in Fig. 12 can be expected to benefit the film-forming ability of the worm/wheel contact by eliminating the unentrained region. In principle, other types of worm may have potential for better film formation and these should be investigated in future work. A contact in which entrainment is 'across' rather than 'along' its main axis would seem to offer some advantage. This suggests a greater degree of conformity between the gear teeth in the direction perpendicular to that of entrainment, as is the case in gears of special design in which the worm teeth have a conforming, concave profile [7].

A significant practical feature that has been ignored in this analysis is that of surface roughness which must be of importance in view of the relatively thin films predicted and the expected finish of worm and wheel surfaces, of the order of 0.5 μm in practice. Significant 'mixed' lubrication or micro EHL effects must therefore be present in real gears, and these effects will be modelled in future work. In view of the relatively low hardness of the wheel material, these effects are likely to take the form of abrasive wear of the wheel in practice. Frictional losses will also be higher as a result of mixed lubrication, and the efficiency figures given in Table 4 are therefore expected to be higher than those that would be measured in practice. Superfinishing of conventional parallel axis gears has been shown to reduce friction by up to 30 per cent [8] and increase the pitting fatigue life by a factor of 4 [9]. It is therefore suggested that improved surface finish, particularly of the harder worm, might be beneficial as a means of reducing both friction and wear. The temperatures above the assumed reference or bulk level that have been calculated arise from the transient frictional heating effect of viscous friction within the contact. These values will also be
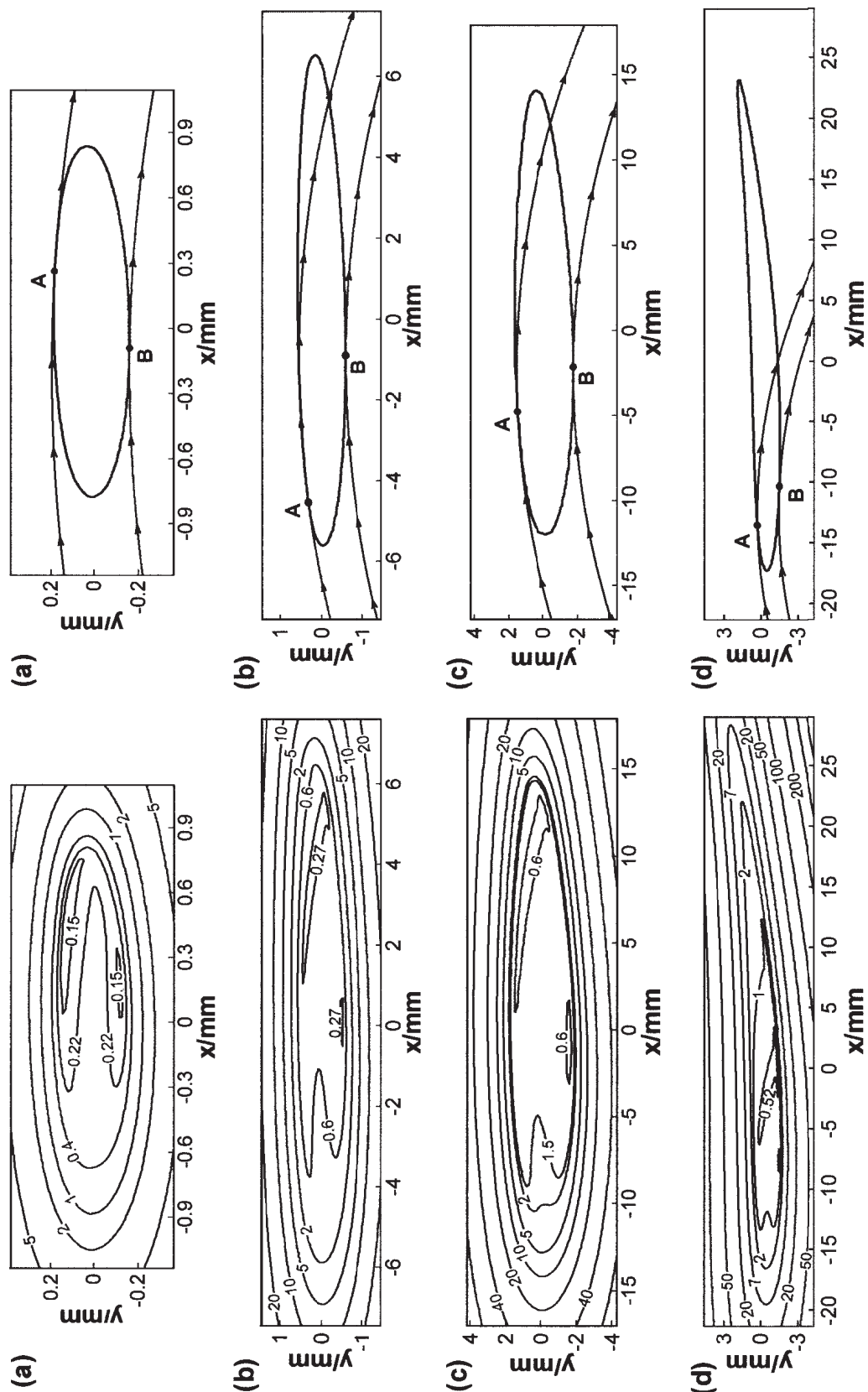
C11400   © IMechE 2001                   Proc Instn Mech Engrs Vol 215 Part C

**Fig. 12**  Comparison of EHL film thickness contours (μm) with lines of poor film forming predicted from dry
contact and entrainment lines that are tangential to the edge of the dry contact: (a) design A; (b)
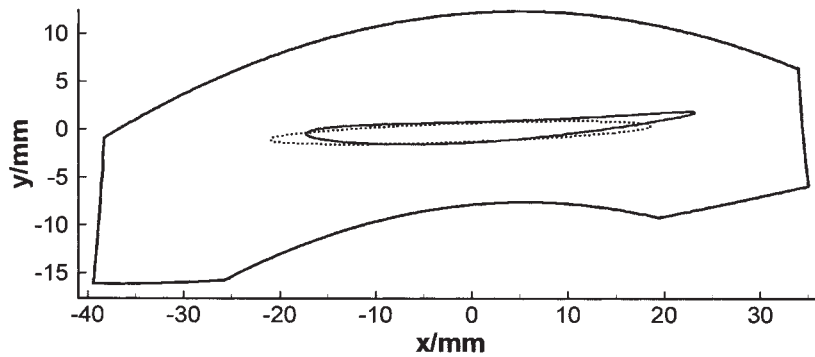design D; (c) design F; (d) design H

**Fig. 13** Comparison of the area of dry contact given by elastic contact simulation (solid line) with that predicted from Hertzian theory (broken line) on the basis of the radii of principal relative curvatures at the contact point (design H)

**Table 5** Comparison of central film thickness values with formulae

| Design | Model | CDDT$_1$ | | CDDT$_2$ | |
|--------|-------|-------|----------------|-------|----------------|
| | | Value | Difference (%) | Value | Difference (%) |
| A | 0.26 | 0.37 | 42 | 0.37 | 43 |
| B | 0.24 | 0.38 | 54 | 0.37 | 53 |
| C | 0.33 | 0.50 | 51 | 0.50 | 49 |
| D | 0.56 | 1.04 | 85 | 1.12 | 99 |
| E | 0.54 | 1.00 | 83 | 1.13 | 107 |
| F | 1.33 | 2.49 | 88 | 2.63 | 98 |
| G | 0.88 | 1.59 | 80 | 1.81 | 106 |
| H | 0.51 | 2.27 | 350 | 1.97 | 290 |

**Table 6** Comparison of minimum film thickness values with formulae

| Design | Model | CDDT$_1$ | | CDDT$_2$ | |
|--------|-------|-------|----------------|-------|----------------|
| | | Value | Difference (%) | Value | Difference (%) |
| A | 0.12 | 0.18 | 54 | 0.18 | 54 |
| B | 0.11 | 0.18 | 62 | 0.18 | 61 |
| C | 0.14 | 0.24 | 72 | 0.24 | 70 |
| D | 0.22 | 0.50 | 122 | 0.54 | 141 |
| E | 0.22 | 0.47 | 120 | 0.54 | 151 |
| F | 0.43 | 1.20 | 181 | 1.28 | 200 |
| G | 0.29 | 0.76 | 161 | 0.89 | 204 |
| H | 0.39 | 1.12 | 190 | 0.95 | 146 |

increased as a result of the inclusion of mixed lubrication effects.

## REFERENCES

**1 Sharif, K. J., Kong, S., Evans, H. P.** and **Snidle, R. W.** Contact and elastohydrodynamic analysis of worm gears. Part 1: theoretical formulation. *Proc. Instn Mech. Engrs*, *Part C*, *Journal of Mechanical Engineering Science*, 2001, **215**(C7), 817–830.

**2** DIN 3975, Terms and definitions for cylindrical worm gears with shaft angle of 90°, Berlin, Germany, 1976.

**3 Hu, J.** The kinematic analysis and metrology of cylindrical worm gearing. PhD thesis, University of Newcastle upon Tyne, 1997.

**4 Larsson, R., Larsson, P. O., Eriksson, E., Sjöberg, M.** and **Höglund, E.** Lubricant properties for input to hydrodynamic and elastohydrodynamic lubrication analyses. *Proc. Instn Mech. Engrs*, *Part J*, *Journal of Engineering Tribology*, 2000, **214**(J1), 17–28.

**5 Yang, F., Su, D.** and **Gentle, C. R.** Mesh stiffness and tooth stress calculation for worm gears using finite element method. In Proceedings of International Conference on *Gearing, Transmissions, and Mechanical Systems*, Nottingham Trent University, July 2000, pp. 129–139 (Professional Engineering Publishing, London).

**6 Chittenden, R. J., Dowson, D., Dunn, J. F.** and **Taylor, C. M.** A theoretical analysis of the isothermal elastohydrodynamic lubrication of concentrated contacts. *Proc. R. Soc. (Lond.) A*, 1985, **397**, 271–294.

**7 Vos, H.** Design measures increase the capacity of worm gear units. *Maschinenmarkt*, February 1996, (8), 56–59.

**8 Britton, R. D., Elcoate, C. D., Alanou, M. P., Evans, H. P.** and **Snidle, R. W.** Effect of surface finish on gear tooth friction. *Trans. ASME*, *J. Tribology*, 2000, **122**, 354–360.

**9 Krantz, T. L., Alanou, M. P., Evans, H. P.** and **Snidle, R. W.** Surface fatigue lives of case-carburized gears with an improved surface finish. *Trans. ASME*, *J. Tribology*, **123** (in press).